Study of the alteration products of a natural uraninite by Raman spectroscopy

L. J. Bonales*, C. Menor-Salván‡, J. Cobos*

*Centro de Investigaciones Energéticas, Medioambientales y Tecnológicas, CIEMAT Avenida Complutense, 40- 28040 – Madrid - Spain

‡Centro de Astrobiología (CSIC-INTA). Ctra. Torrejón-Ajalvir, km 4- 28850-Torrejon de Ardoz - Spain.

CORRESPONDING AUTHOR

laura.jimenez@ciemat.es

Centro de Investigaciones Energéticas, Medioambientales y Tecnológicas, CIEMAT. Departamento de Energía. Unidad de Residuos de Alta Actividad.

Av Complutense, 40, 28040 Madrid, Spain

Telephone number: + 34 913462576

ABSTRACT

Uraninite is a mineral considered as an analogue of the spent fuel, and the study of its alteration products has been used to predict the secondary phases produced during the fuel storage under specific environmental conditions. In this work, we study by Raman spectroscopy the alteration by weathering of the primary uraninite from the uranium deposit of Sierra Albarrana. Beside the identification of the different secondary phases, based on the analysis of the symmetrical stretching vibration of the uranyl group (UO_2^{2+}), which allows the identification of individual uranyl phases and can be used as a fingerprint. We show in this work a new approach to perform a pseudo-quantitative analysis of these uranium minerals by means of Raman spectroscopy.

KEYWORDS

Spent fuel, uraninite, natural analogue, secondary phases, Raman spectroscopy.

1. INTRODUCTION

It is widely accepted that spent nuclear fuel (SNF) will be disposed in an underground repository. After storage times of the order of some thousand years, it is expected that the spent fuel will be exposed to groundwater, when the containers surrounding the waste may be breachedIdentification of the reaction products generated.by the interaction of the waste form with water is required to characterize the repository performance [1].

All scenarios describing the spent fuel-groundwater contact require extrapolations to the far future of a complex system, whose components are not all well defined. It is expected that the conditions in a spent fuel deep geological disposal will be reducing. Nevertheless oxidizing species near to the spent fuel surface will increase caused by radiolysis of water due to the ionizing radiation associated with the fuel will increase[2, J. Cobos2,*, L.Havela1, V. V. Rondinella1, J.De Pablo3, T. Gouder1, J. P. Glatz1, P. Carbol1 and H. Matzke1, Radiochim. Acta **90**, 597–602 (2002)], which is dominated at the predicted time of the breached containers by the α-decay [3,4,Cobos, J., Matzke, H., Rondinella, V. V., Martinez-Esparza, A.,Wiss, T.: Proc. GLOBAL '99 Int. Conf. on Future Nuclear Systems, Aug. 29–Sept. 3 (1999) Jackson Hole, USA, A.N.S.]. In particular, only those radiolysis products, which are formed in the water layer near the fuel surface, *i.e*. within <50 μm of the fuel surface, are effective in causing the fuel oxidation [5]. Therefore, both dissolution and precipitation processes under this conditions will affect the overall behavior of the fuel matrix. Depending of the surface / volume ratio, secondary phases will appear on the spent fuel surface as alteration products [6,J. Cobos2,□, L.Havela1, V. V. Rondinella1, J.De Pablo3, T. Gouder1, J. P. Glatz1, P. Carbol1 and H. Matzke1, Radiochim. Acta 90, 597–602 (2002)].

Different approaches can be done in order to study the dissolution/precipitation processes of spent nuclear fuel (SF) and understand the potential migration of uranium under repository conditions after millions of years. On one hand, the use of mathematical models [7,8]predict SF behavior in the long-term and expected conditions. These

theoretical methods require the knowledge of physico-chemical parameters. These must be obtained experimentally in laboratory assays for SF analogues, such as uranium dioxide UO_2 [9,10] or SIMFUEL [11,12]. On the other hand, the studies of natural analogues have been very successful, to understand different aspects of the SF corrosion processes at longer storage times [13-24].

The uraninite is known as the natural analogue of the SF, and studies about its dissolution [13,14] and its corrosion [15,16] at different conditions have been performed from decades. The consideration of this mineral as an analogue of the SF is mainly due to two reasons: 1) the chemical composition of uraninite and spent fuel is very similar, (UO_2 > 95 %) [17,18], 2) both materials have a cubic fluorite structure, (space group #225 Fm3m).Studies of different uraninites has been widely performed. . Some works [19,20,21,22] have been shown the sequence of the alteration products of natural uraninites at different geochemistry conditions. The general trend of this sequence was previously recognized by Frondel [23,24] and it is still widely accepted as: 1) uranium oxides, 2) uranyl oxyhydroxides and 3) uranyl silicates, and the specific alteration products depend on local conditions.

This work focuses on the complete identification by Raman spectroscopy of the supergenic uranyl phases produced by alteration of a natural analogue of the spent fuel: the uraninite from Sierra Albarrana (Spain). This is the first study of uraninite and its associated secondary uranium minerals from the uranium deposit of Sierra Albarrana, and it has been shown that the complete characterization of uranium secondary phases is possible using only one characterization technique. Emphasis on the development of a new approach, the pseudo-quantitative analysis of these uranium minerals by Raman spectroscopy has been done.

2. MATERIALS AND METHODS

2.1. Mineral sample and geological setting

The sample studied is a "uraninite + gummite" from Sierra Albarrana (Córdoba, Spain), kindly provided by the Museum of Natural Sciences of Alava (Vitoria, Spain). It has been collected during the uranium extractive activity in 1960.

The sample structure corresponds to the ideal gummite occurrence [23, 24] (see Fig.1.a): a veined central core black to brownish black and yellow to orange or greenish yellow surrounding zone, vitreous to dull or earthy, formed by several supergenic minerals.

The uranium-rare earth mineralization at Sierra Albarrana (Cordoba, Spain) [25] is distributed in a complex pegmatite field of granitic composition. The pegmatites are not related with plutonic bodies and are syn-metamorphic and formed by anatexis associated to medium to high grade metamorphism during Variscan. The pegmatite field is hosted by the Cambrian quartzite and gneiss of the metamorphic nucleus of the Albarrana formation [26]. The pegmatite form irregular bodies and veins parallel to the Variscan structures. The pegmatite mineralogy is controlled by the metamorphic grade and the accessory minerals include uraninite, thorite, brannerite, beryl, schorl , rutile, ilmenite, allanite-(Ce), zircon, monazite-(Ce), xenotime, columbite-tantalite, chrysoberyl and Fe-Mn-Mg-Caphosphates [27,28]. From a geochemical point of view, the uraninite-gummite samples studied in this work belong to a pegmatite of the Muscovite-rare element class in the Cherny classification [29] and the type "Dieresis" in the classification of Gonzalez del Tánago [30], hosted by rich biotitic-muscovitic gneisses. This type of pegmatite was worked for the extraction of uranium.

2.2.Preparation of the sample

The sample studied in this work was obtained from the Mineralogy collection of the Natural Sciences Museum of Alava (MCNA, Vitoria, Spain). The sample is from the *Dieresis* uranium mine (Sierra Albarrana, Córdoba, Spain)

The sample was cut using a diamond saw and polished. The thick polished sections obtained were subjected to spectroscopic analysis.

2.3.SEM-EDS

A polished section of the sample were analysed under a Jeol 5600-LV scanning electron microscope equipped with an Oxford Industries INCA X-sight energy dispersive X-ray spectrometer. Backscattered electron images and energy dispersive spectra were obtained on the sample mounted on Al stubs and without coating (V=20 kV I=85 μA, electron beam diameter 1 μm).

2.4.Raman spectroscopy technique

The Raman spectroscopy was carried out using a Horiba LabRam HR evolution spectrometer (Jobin Yvon Technology). A red laser of HeNe with a wavelength of 632.81 nm and an operation power of 20mW was used as the excitation source. The laser was focused onto the sample using 20x objective at the confocal microscope BX4 with confocal 800mm; the scatter light was collected with the same objective and then dispersed with a a Jobin-Yvon spectrometer (600 gooves / mm), and detected with a peltier cooled CCD detector (256 x1024 pix.). The spectral resolution was about 1 cm^{-1} per pixel.

2.5.Raman mapping procedure

The surface of the sample was analyzed by acquiring 100 spectra in different points separated 100 μm from each other. The first one corresponds to the center of the sample and the rest were located on a line going from the center of the sample outwards, (see Fig1a,b). The protocol used is a combination of the line-mapping and step-by-step procedures, as described below:

The sample is placed in the motorized x – y stage under the microscope objective and focused on the center. Then, a line-mapping is performed using the automatized line-scanning tool. This tool allows the acquisition of a complete Raman spectrum at different points on a line by automatically moving the stage in one or two directions (x – y).

The microscope objective used in this work, with a magnification of 20x, allows the visualization of a maximum area of 500 μm x 70 μm (Figure 1c). Therefore, in order to analyze the whole sample (10 mm) 20 lines with 5 equidistant points each have been measured. This was performed with the step-by-step procedure, in which the motorized stage is moved 500 μm (the line-mapping length) in the x direction to allow the analysis of the next part of the sample.

The acquisition time for each spectrum was ~100 s on an extended shift of 100 - 1200 cm^{-1}. During the start of all Raman scan, a cosmic ray subtraction is automatically carried out to count any radioactive interference from the atmosphere or the sample. All spectra were re-calibrated daily with the emission lines of a Ne lamp. Spectra manipulation such as baseline adjustment, smoothing, and normalization was performed using the Origin software. Spectral analyses were performance by comparison with spectra from an in-house library as well as a commercially available spectral library (RRUFF database [31]).

3. RESULTS AND DISCUSION

By using the Raman line-mapping procedure described before, we had achieved the results which can be divided in three parts: identification of the different secondary phases by using the Raman finger-print, analysis of the different regions and pseudo-quantitative analysis of the sample. The results obtained are coherent with the SEM-EDS study of the texture of the sample.

3.1. SEM-EDS analysis

The texture of the uranium ore sample in polished section shows an alteration rim in contact with unaltered uraninite constituted by phase composed by U, O and C (Fig. 2b), unidentifiable by EDS spectroscopy. The same secondary phase was found filling small fractures in the relicts of unaltered uraninite. The outer part of the altered uraninite is composed by a yellow secondary phase containing calcium, uranium and silicon, as can be seen in the Fig. 2c. The Fig. 2d shows an irregular grains and inclusions containing lead, uranium and silicon. The microscopic observation of the texture suggest a first stage of uraninite alteration, characterized by the formation of oxide-carbonate phases and a second phase This phase is characterized by the reaction with silica and calcium, rich fluids that affects the external zone of the sample, with formation of uranyl silicate phases. The exolution of radiogenic lead was observed by the formation of a separate lead bearing silicate phase.

The Raman analysis of the sample is necessary to complete the fully characterization of the secondary mineral assemblage, as the EDS spectroscopy is unable to define the mineral phases observed, especially during the first stages of alteration of primary uraninite.

3.2. Identification of the secondary phases

By scanning the sample with the Raman technique from the center outwards, four secondary uranium phases beyond uraninite were identified: rutherfordine, $UO_2(CO_3)$, soddyite, $(UO_2)_2SiO_4•2H_2O$, uranophane alpha $Ca(UO_2)_2(SiO_3OH)_2•5H_2O$ and kasolite, $PbUO_2SiO_4•H_2O$, see spectra shown in Figure 3.

Rutherfordine was identified by means of the two symmetric stretching bands, ν_1, characterized at 889 cm^{-1} and 1120 cm^{-1} of the $(UO_2)^{2+}$ and $(CO_3)^{2-}$ groups, respectively. The band at 830 cm^{-1}, is attributable to the ν_2 bending modes of the $(CO_3)^{2-}$ group, $\nu_2(CO_3)^{2-}$, and the band with lower intensity at 789 cm^{-1} is due to the ν_4 out of plane bending modes. In the low wavenumber region, those bands at ~142 cm^{-1}, 162 cm^{-1} and 220 cm^{-1}, may be assigned to the lattice vibrations [32].

The uranyl silicate minerals found in the sample: uranophane alpha, $Ca(UO_2)_2(SiO_3OH)_2•5H_2O$, soddyite, $(UO_2)_2SiO_4•2H_2O$, and kasolite $PbUO_2SiO_4•H_2O$, were identified using the two internal modes ν_1 of the $(UO_2)^{2+}$ and $(SiO_4)^{4-}$. Symmetric stretching mode, $\nu_1(UO_2)^{2+}$ at 798 cm^{-1} and $\nu_1(SiO_4)^{4-}$ at 967 cm^{-1} correspond to uranophane alpha and the expected overlapping of these bands, $\nu_1(UO_2)^{2+}$ and $\nu_1(SiO_4)^{4-}$, at 832 cm^{-1} indicate soddyite. The Raman spectrum of kasolite has been characterized by the bands at 768 cm^{-1} and 912 cm^{-1}, corresponding to the symmetric stretching modes $\nu_1(UO_2)^{2+}$ and $\nu_1(SiO_4)^{4-}$ respectively, and the bands at 949 cm^{-1} and 972 cm^{-1} correspond to the $\nu_3(SiO_4)^{4-}$ bending modes. For the three uranyl silicates, the bands into the low wavenumber region, 200 - 300 cm^{-1} are assigned to ν_2 bending modes of $(UO_2)^{2+}$, whereas bands corresponding to the bending modes of $(SiO_4)^{4-}$, ν_2 and ν_4, appears at ~ 400 cm^{-1} and 450 - 600 cm^{-1}, respectively [33,34].

The assignation to the different vibration modes of each phase are shown in Table 1, 2 3 and 4. The peak positions are in good agreement with the published literature values

[32~~36~~, 33~~37~~, 34~~38~~, 35] and standard materials [31~~35~~]. The fingerprint used in this work to identify each phase in the sample was the symmetrical stretching vibration of the UO_2^{2+} group, $\nu_1(UO_2)^{2+}$. As it can be seen in the in Figure 3, these bands are well resolved and do not overlap each other(frequencies indicated in bold in Tables 1, 2, 3 and 4).

3.3.Region analysis

The distribution of the different phases along the sample can be divided into eight regions from the center outwards (see Fig, 1b), where a phase or a mixture of two or more phases predominates over the others.

3.3.1. Region 1, 2 and 3

The region 1 covers approximately from the center of the sample (0 mm) to 0.4 mm and is considered the core of the sample, comprising uraninite (UO_{2+x}), without any alteration products. The region 2 (0.4 – 0.8 mm) is characterized by the presence of soddyite and the region 3 (0.8 – 1.0 mm) corresponds to a mixture of soddyite and rutherfordine (spectra at 0.8 and 0.9). Fig.4 shows the Raman spectra obtained in region 2 and 3 at 0.8 and 0.9 mm from the center, of the sample respectively. Soddyite has been identified in the region 2 and a mixture of soddyite and rutherfordine in region 3.

3.3.2. Region 4

In Figure 5 can be observed the region 4 (1.0 – 3.3 mm) characterized by the coexistence of the four secondary phases, soddyite, rutherfordine, uranophane alpha and kasolite in different proportions.. The proportions of the different phases in the mixtures can be compared by the analysis of the different relative intensities of the spectra bands. As it is well known, Raman spectroscopy can be used as an analytical technique to extract quantitative information [36]. The intensity of Raman scattering, I_R, can be written as

$$I_R = (I_L \sigma \eta P)\, C, \quad (1)$$

where I_L is the laser intensity, σ is the Raman cross-section or scattering efficiency, η is an instrument parameter, P is the sample path length, and C is the concentration [37]. Therefore, intensity peak ratios (I_A / I_B) may be used to determine relative concentrations $R_{CA/CB}$ of two components, A and B; thus, $R_{CA/CB} = C_A / C_B$, where C_A and C_B are the concentrations of A and B, respectively.

By using the different peak ratios one can conclude that the spectra acquired at 1.7 and 1.3 mm shown in Figure 5 correspond to mixtures of these four phases where the amount of soddyite is higher than in the mixture corresponding to spectra acquired at 1.6 mm; *i.e.* the relative intensity of the band $\nu_1(UO_2)^{2+}$ of soddyite, $I_{v1(soddyite)}$, in relation to the band intensities of the $\nu_1(UO_2)^{2+}$ of the others minerals, $I_{v1(rutherfordine)}$, $I_{v1(uranophane\ alpha)}$, and $I_{v1(kasolite)}$, is higher in the spectra at 1.7 and 1.3 mm than in the spectra corresponding to 1.6 mm.

3.3.3. Region 5 and 6

Figure 6 shows the typical spectra found in region 5 (3.3 - 4.6 mm) and 6 (4.6 -7.1 mm). In these two regions, from 3.3 mm to the center of the sample, the uranyl carbonate, identified as rutherfordine, was completely consumed and substituted by uranyl silicates, such as soddyite and uranophane alpha in region 5, These silicates, has been identified as kasolite in the region 6. The analysis of the relative intensities in these regions indicates different proportions of the different phases in the sample. Figure 6a shows the mixture corresponding to the spectrum at 3.8 mm, it has a relation of soddyite / uranophane alpha higher than the mixtures of the spectra at 3.6 and 3.7 mm. Moreover the mixture corresponding to the spectrum at 4.7 mm shown in Fig. 6b is a mixture richer in kasolite than in the others mixtures.

3.3.4. Region 7 and 8

In Figure 7 the spectra analyzed in region 7 (7.1 mm – 8.8 mm) and 8 (8.8 – 1.0 mm) are shown. In these two outer regions the predominant phase is uranophane alpha, being this the only phase present in region 7, while in region 8 this phase coexists with kasolite at different proportions. As it can be seen in Figures 4, 5, 6 and 7, most of the Raman spectra acquired in this work correspond to mixtures of different phases in which the fraction of the different minerals is highly variable, very typical of gummites as expected.

3.4. Pseudo - quantitative analysis

In order to perform a pseudo - quantitative analysis of the sample in order to identifythe presence or absence of different phases along the different regions of gummite (from 0.4 to 10.00 mm), it has been processed 100 spectra analized as follow. This analysis is based on a characteristic of Raman spectra for mixtures: the spectra can be understood as the direct sum of the individual spectrum of each component in the mixture as long as these components do not interact with each other. Therefore, the vibration bands do not undergo any displacement, and the band profile of the mixture spectra results in the spectra of the different components or *vice versa*. In order to calculate the number of contributions of a given band, which is not always detectable to the naked eye, it has been analyzed the resulting spectrum by the second derivate method [38]. The first derivative gives us an idea of the number of contributions involved but, as usual in spectroscopy, is the second derivative which enables us to determine the number of contributions, since each one leads to a minimum. As an example, in Figure 8, the analysis of the second derivative of the $\nu_1(UO_2)^{2+}$ stretch region at 700 - 900cm^{-1} is shown. This figure highlights that when the amount of a phase in a mixture is very small, in proportion to the other present phases, it is necessary to perform the analysis of the second derivative to identify the number of

contributions, (Fig. 8), since the band corresponding to a lower amount appears as a shoulder, and not as a resolved peak. Thereby, we determine the number of contributions by calculating the second derivate of each spectrum and by constructing a data matrix of 0 and 1, where 0 means there is no minimum to the characteristic frequency of the mineral, and 1 if there is a minimum at the characteristic frequency of the mineral.

Figure 9 shows the diagrams constructed by this method*, i.e.* we plot the presence (1) or absence (0) for each phase *vs.* position of the analyzed point, from the center of the sample outwards (0 -10 mm). Lines are the smoothed data and indicate the trends of increase or decrease of each phase along the sample.

As it can be seen in Figure 9, the center of the sample, 0 – 0.4 mm, is composed by uraninite. The rutherfordine is the predominant phase in the inner part, 0.4 – 3.3 mm, in contact with the uraninite core, and then is absent from 3.3 mm. The analysis of the next region indicates a mixture of uranyl silicates: soddyite, uranophane alpha and kasolite. Soddyite prevails in the inner part, 0.4 – 7.1 mm; uranophane alpha predominates in the outer part of the sample, 7.1 – 10 mm, and kasolite appears intermittently (1.0 - 3.3 mm; 4.6 - 7.1 mm and 8.8 – 10 mm).

It should be note that schoepite, $(UO_2)_4O(OH)_6 \bullet 6H_2O$, the expected uranyl phase formed by corrosion of uraninite under atmospheric conditions [15] or by silica-poor meteoric waters, has not been observed in the sample analyzed in this work. The absence of a significant occurrence of schoepite in the sample could be explained by its rapid transformation, to rutherfordine, which appears as replacement structures in the gummite rim, suggesting that the original schoepite or metaschoepite has been replaced by the rutherfordine, as it is the stable phase in CO_2 rich fluids in subsurface conditions [43].

The formation of rutherfordine, confined in the inner zone of the corrosion rim of uraninite, could be one of the first steps of alteration, after the formation of the schoepite or metaschoepite or other oxy-hydroxydes with different U(IV)-U(IV) proportion.

The next alteration products are the uranyl silicates soddyite and uranophane alpha. Soddyite is the first silicate precipitate by reaction of silicate rich solutions with uraninite and the first alteration product, replacing them in the vicinity of the primary mineral. The formation of soddyite or uranophane depends on the activity ratio (Ca)/(H+). As a result, Ca poor and low pH waters favor the replacement of schoepite by soddyite [39].

The formation of uranophane alpha requires a calcium and silica rich fluid, provided by the alteration of the feldspars (mainly plagioclases) that usually surround the uraninite crystals in the pegmatite [34].

Hence, the circulant calcium and silica rich water determines de distribution of silicates in the gummite. The external zone of the corrosion rim, in contact with altered feldspars, is almost entirely composed by uranophane and the inner zone and contacts with uraninite, more U rich and Ca poor, are dominated by soddyite. The mineral assemblage, in presence of persisting uraninite, is determined by the composition of infiltrating waters.

An interesting feature of our sample is the lead enrichment in the form of kasolite in the gummite zone. The accumulation of lead in the uraninite destabilizes its structure by induction of strain. Under oxidizing conditions, lead combine with uranyl to form Pb-uranyl minerals. Lead is not incorporated to rutherfordine, soddyite and uranophane however kasolite accumulates in fractures and veinlets. The role of radiogenic Pb is essential in the formation of secondary phases. The formation of vandendriesscheite, coetaneous with the formation of schoepite, alters incongruently in presence of CO_2

waters to form uranyl carbonates and lead enriched phases, as masuyite, whose alteration in silica rich waters lead to the formation of kasolite. The lower mobility of Pb mineral phases compared with uranyl phases lead to a gradual enrichment in kasolite on the gummite.

4. CONCLUSION

In this work we present the Raman spectra of the alteration products of a uraninite sample, (an analogue of the spent fuel), taken from the Sierra Albarrana, Spain. The identification of the different secondary phases, have been performed by the analysis of the symmetrical stretching vibration of the uranyl group (UO_2^{2+}), taken as fingerprint of the found phases: rutherfordine, $UO_2(CO_3)$, soddyite, $(UO_2)_2SiO_4 \bullet 2H_2O$, uranophane alpha $Ca(UO_2)_2(SiO_3OH)2 \bullet 5H_2O$ and kasolite, $PbUO_2SiO_4 \bullet H_2O$. The sequence of alteration products obtained was: 1) uraninite constitutes the core of the sample, 0 – 0.4 mm. 2) Rutherfordine appears in the inner part, 0.4 – 3.3 mm, in contact with the uraninite core. 3) A mixture of uranyl silicates: soddyite, uranophane alpha and kasolite. Soddyite prevails in the inner part, 0.4 – 7.1 mm; uranophane alpha predominates in the outer part of the sample, 7.1 – 10 mm, and kasolite appears intermittently (1.0 - 3.3 mm; 4.6 - 7.1 mm and 8.8 – 10 mm). This sequence had been obtained by using a pseudo-quantitative analysis developed in this work, which enable to elucidate the presence or absence of the different phases in an easy and quick way and moreover, without using other complementary techniques.

Schoepite, $(UO_2)_4O(OH)_6 \bullet 6H_2O$, the expected uranyl phase formed by corrosion of uraninite under atmospheric conditions has not been observed due to its rapid transformation, to rutherfordine, which appears as replacement structures in the gummite rim.

Because the knowledge of Raman spectra of uranyl-based minerals is still rather limited, this study, as a part of our ongoing research into the use of Raman spectroscopy, intend to increase the Raman database spectra of uranium based-minerals, as important in the field of nuclear waste disposal.

5. ACKNOWLEDGMENTS

Authors thank to Jose González del Tánago for many useful comments and to the Museo de Ciencias Naturales de Alava for kindly providing the samples used in this study. This work was supported by ENRESA in the project: Nº 079000189 entitle "Aplicación de técnicas de caracterización en el estudio de la estabilidad del combustible nuclear irradiado en condiciones de almacenamiento" (ACESCO).

6. REFERENCES

[1] SKB 91, Final Disposal of spent nuclear fuel. Importance of the bedrock for safety, SKB Report 92-20 (May 1992).

[2] D.W. Shoesmith, J. Nucl. Mater. 282 (2000) 1-31.

[3] S. Sunder, Nucl. Tech. 122 (1998) 211-221.

[4] A.O. Allen, The Radiation Chemistry of Water and Aqueous Solutions", D. Van Nostrand Co. Inc, Princeton, 1961

[5] H. Christensen and S. Sunder, J. Nucl. Mater. 238 (1996) 70-77.

[6] R. Wang, and J. B. Katayama, Nucl. Chem. Wast. Manag. 3 (1982) 83-90.

[7] J. Bruno, E. Cera, L. Duro, T.E. Eriksen, L.O. Werme, J. Nucl. Mater. 238 (1996) 110-120.

[8] J. de Pablo, I. Casas, J. Giménez, V. Marti, M. E. Torrero. J. Nucl. Mater. 232 (1996) 138-145.

[9] Casas I., Giménez J., Martí V., Torrero M. E., J. de Pablo, Radiochim. Acta, 66-67, (1994), 23-27.

[10] P. Fors, P. Carbol, S. Van Winckel, K. Spahiu, J. Nucl. Mater. 394 (2009) 1-8.

[11] J. Bruno, I. Casas, M.C.A. Sandino, J. Nucl. Mater. 190 (1992) 61-69.

[12] K. Ollila, J. Nucl. Mater. 190 (1992) 70-77.

[13] D.E. Grandstaff, Econ. Geol. 71, (1976) 1493-1506.

[14] J. Janeczek and R.C. Ewing, J. Nucl. Mater. 190 (1992) 157–173.

[15] R.J. Finch and R.C. Ewing, J. Nucl. Mater. 190 (1992) 133–156.

[16] J. Janeczek and R. C. Ewing, J. Nucl. Mater. 185 (1991) 66–77.

[17] J. Janeczek, R.C. Ewing Janeczek, , J. Nucl. Mater. 190 (1992) 128-132.

[18] J. Janeczek, R.C. Ewing, V.M. Oversby, L.O. Werme, J. Nucl. Mater. 238 (1996) 121-130.

[19] E.C. Pearcy, J. D. Prikryl, W.M. Murphy, B.W. Leslie, App. Geochem. 9 (1994) 713-732.

[20] D. Zhao, R.C. Ewing, Radiochimica Acta, 88 (2000) 739-749.

[21] A. P. Deditius, S. Utsunomiya, R.C. Ewing, Geochimica et Cosmochimica Acta, 71 (2007) 4954-4973.

[22] L. Perez del Villar, J, Bruno, R. Campos, P.Gomez, J.S. Cozar, A. Garralon, B. Buil, D. Arcos, G. Carretero, J. Ruiz Sanchez-Porro, P. Hernan, Chemical Gelogy 190 (2002) 395-415.

[23] C. Frondel, US Geol. Surv. Bull. 1064 (1958).

[24] C. Frondel, Am. Mineral. 41 (1956) 539-568.

[25]J. González del Tánago, M. Martinez, , M. Peinado, I Congreso español de Geología, II, (1984) 131-145.

[26] F. Tornos, C.M.C Inverno, C. Casquet, A. Mateus, G. Ortiz, V. Oliveira, Journal of Iberian Geology 30 (2004) 143-181.

[27] J. González del Tánago, Boletín Sociedad Española de Mineralogía, 14-1 (1991), 54-55.

[28] J. González del Tánago, M. Peinado, J.L. Brändle, Boletín Sociedad Española de Mineralogía, 14-1 (1991) 105-106.

[29] Cherny, P., Ercit, T.S. Can. Mineral. 43 (2005) 2005-2026 .

[30] J. González del Tánago,. PhD. Thesis. Universidad Complutense de Madrid (1993).

[31] R.T. Downs (2006) The RRUFF Project: an integrated study of the chemistry, crystallography, Raman and infrared spectroscopy of minerals. Program and Abstracts of the 19th General Meeting of the International Mineralogical Association in Kobe, Japan. O03-13.

[32] R.L. Frost, C. Jiri, J. Raman Spectrosc. 40 (2009) 1096-1103.

[33] R.L. Frost, J.Cejka, M. L. Weier, W. Martens J. Raman Spectrosc. 37 (2006) 538-551.

[34] R.L. Frost, M.L. Weier, W. Martens, T. Kloprogge, J. Cejka, Spectrochimica Acta 63 (2006) 305-312.

[35] B.M. Biwer, W. L. Ebert, J. K. Bates, J. Nucl. Mater. 175 (1990) 188-193.

[36] J.D. Pasteris, B. Wopenka and J.C. Seitz, Geochim. Cosmochim. Acta 52 (1988) 979-988.

[37] S. White, Applied Spectroscopy 67 (2010) 819-827.

[38] E. del Corro García, pHD Thesis. Universidad Complutense de Madrid. CC. Químicas Departamento de Química Física I. (2011)

[39] R. Finch, T. Murakami, Reviews in mineralogy 38 (1999) 91-179.

Figures:

Figure 1

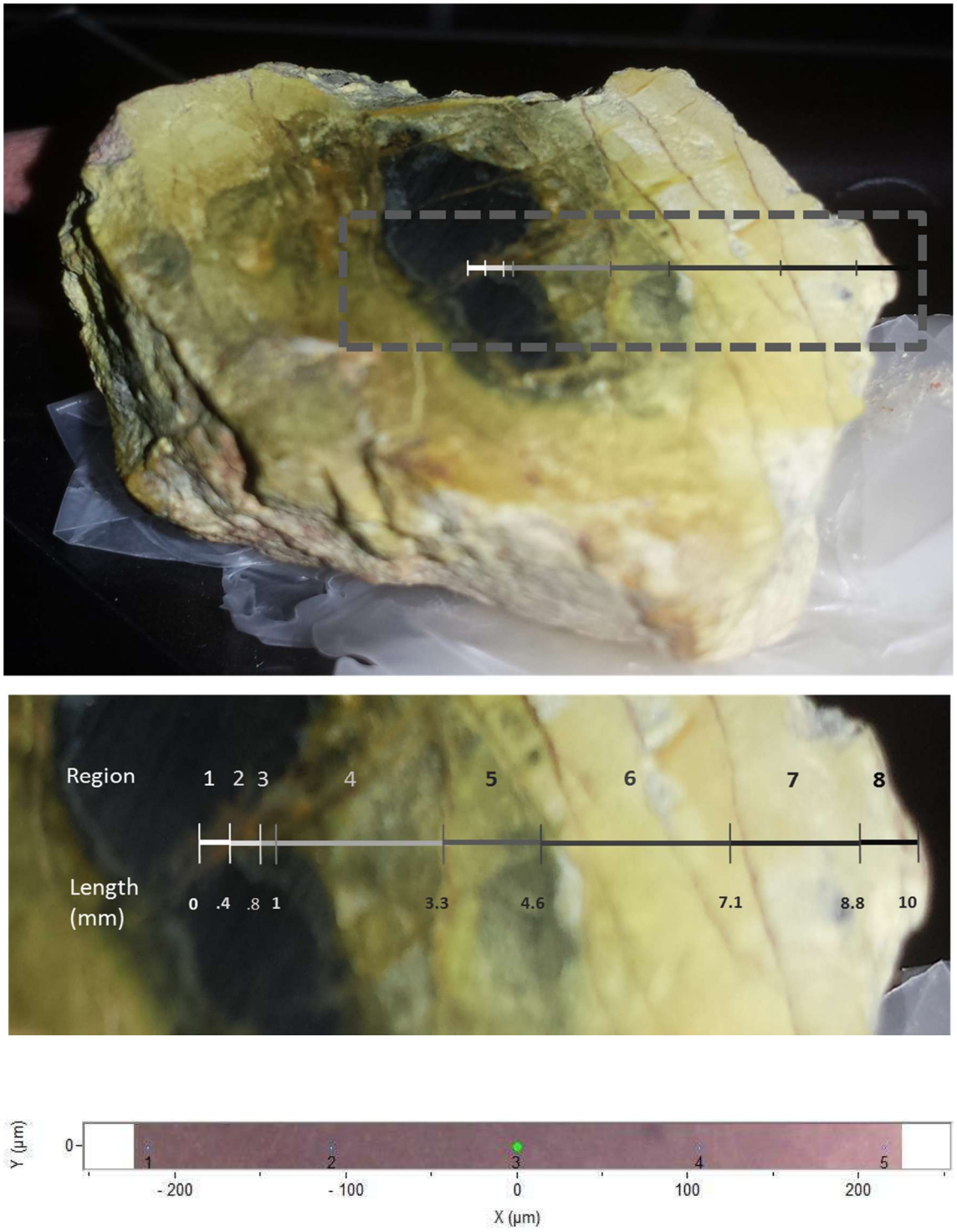

Fig. 1 a) Macro-photograph of the studied sample. b) Macro-photograph of the different regions analyzed. c) Optical microscopy of the first line-mapping.

Figure 2

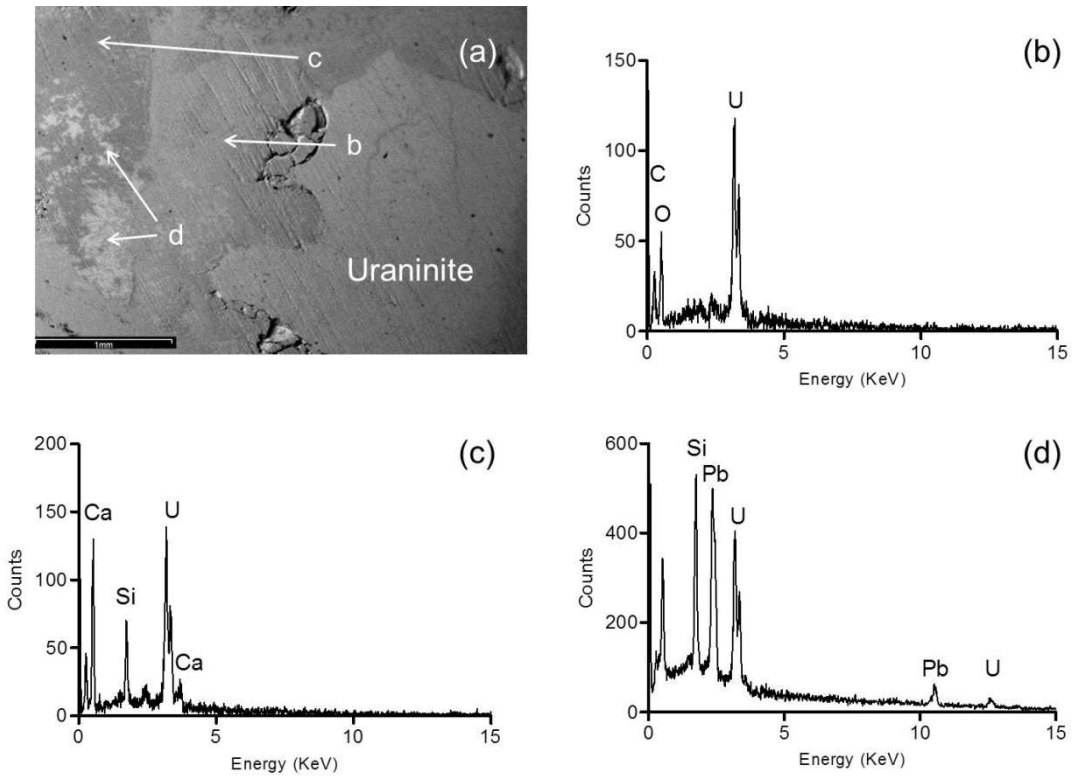

Fig. 2 (a) Backscattered electron image of a section of uraninite sample showing alteration sequence to oxidized uranium phase. (b) EDS spectrum of the oxide-carbonate alteration product. (c) EDS spectrum of uranyl, calcium and silicate rich alteration zone that constitutes the main supergenic phase. (d) EDS spectrum of intergrown uranyl and lead silicate phase.

Figure 3

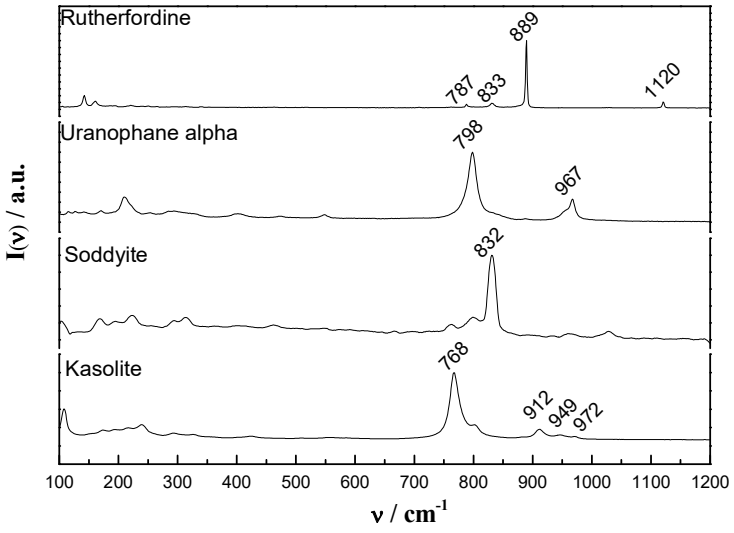

Fig. 3 Raman spectra of the four secondary uranium phases identified: rutherfordine, $UO_2(CO_3)$, uranophane alpha $Ca(UO_2)_2(SiO_3OH)_2 \bullet 5H_2O$, soddyite, $(UO_2)_2SiO_4 \bullet 2H_2O$, and kasolite, $PbUO_2SiO_4 \bullet H_2O$.

Figure 4

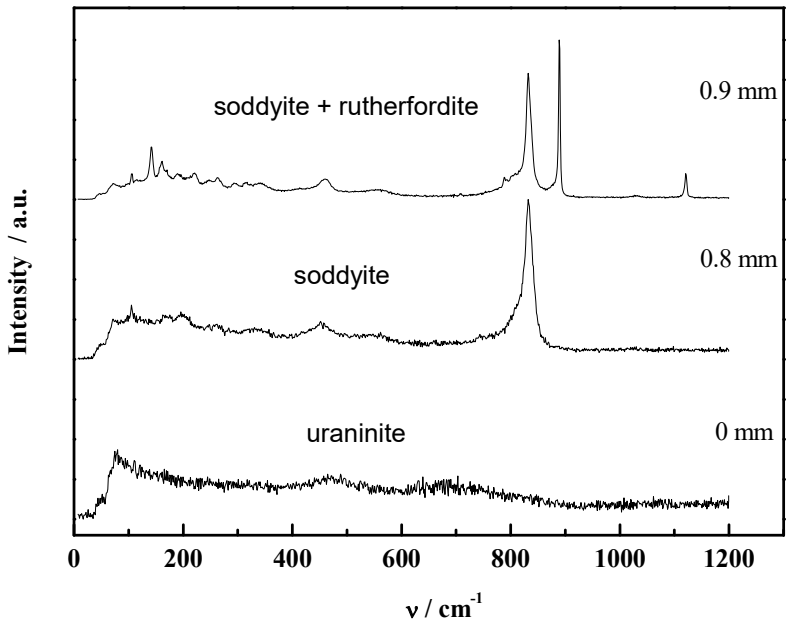

Fig.4 Raman spectra obtained in region 2 and 3 at 0.8 and 0.9 mm from the center, of the sample respectively which show soddyite for region 2 and a mixture of soddyite and rutherfordine in region 3.

Figure 5

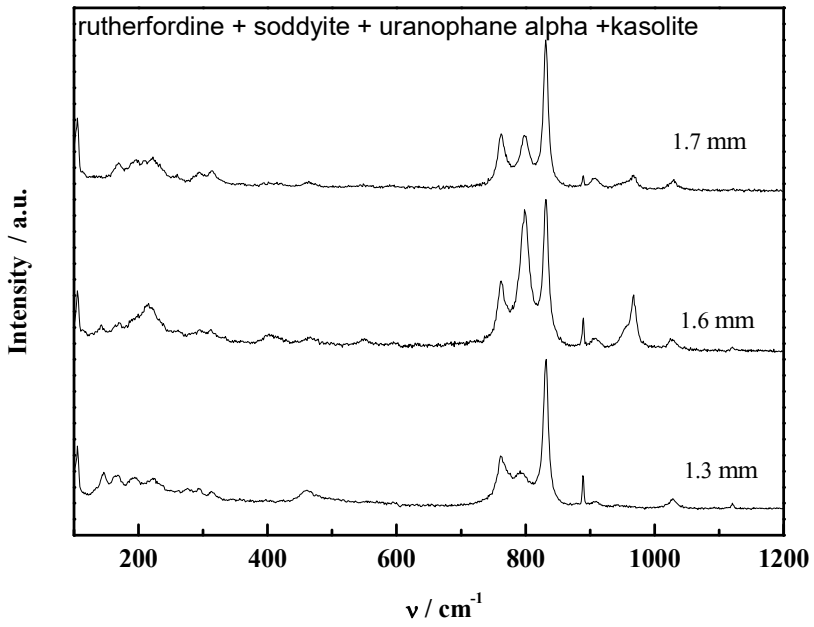

Fig.5 Raman spectra obtained in region 4 at 1.3, 1.6 and 1.7 mm from the center of the sample, which show a mixture of rutherfordine, soddyite, uranophane alpha and kasolite.

Figure 6

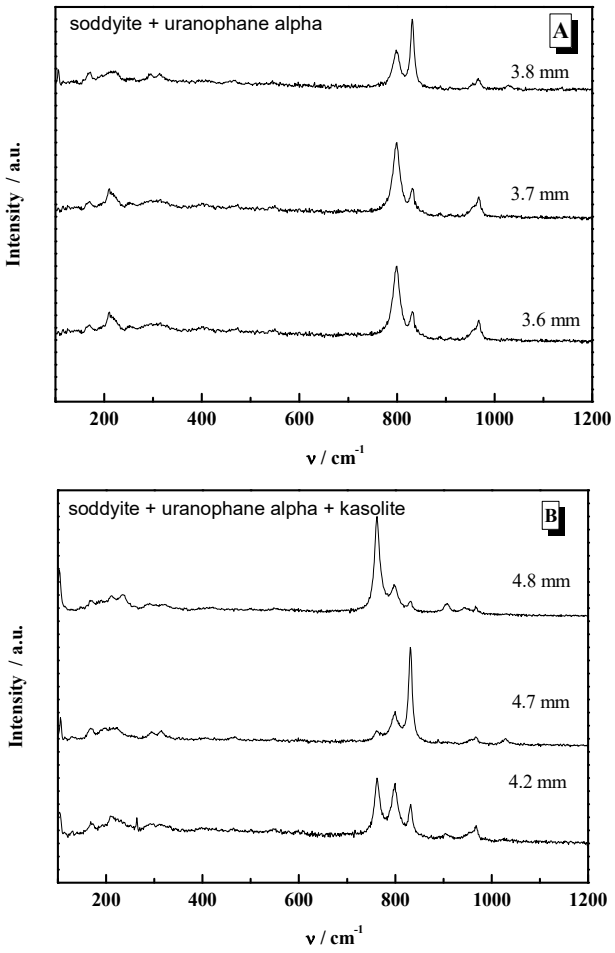

Fig. 6 (a) Raman spectra obtained in region 5 at 3.6, 3.7 and 3.8 mm from the center of the sample which show the characteristic bands of the soddyite and uranophane alpha mixture. (b) Raman spectra obtained in region 6 at 4.2, 4.7 and 4.8 mm from the center of the sample which show a mixture of soddyite, uranophane alpha and kasolite.

Figure 7

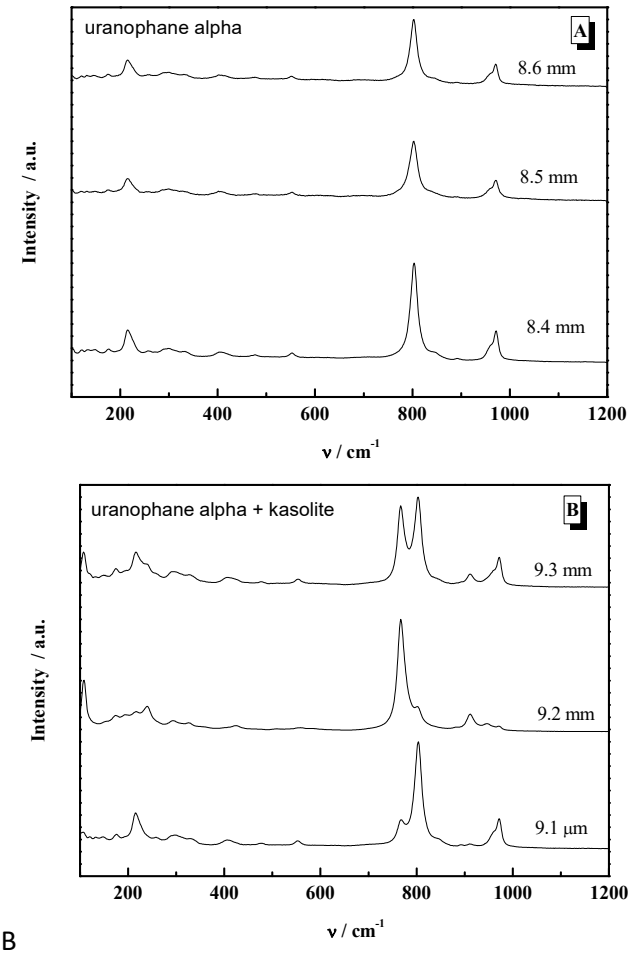

B

Fig. 7 (a) Raman spectra obtained in region 7 at 8.4, 8.5 and 8.6 mm from the center of the sample which show the characteristic spectra of uranophane alpha. (b) Raman spectra obtained in region 8 at 9.1, 9.2 and 9.3 mm from the center of the sample which show a mixture of uranophane alpha and soddyite.

Figure 8

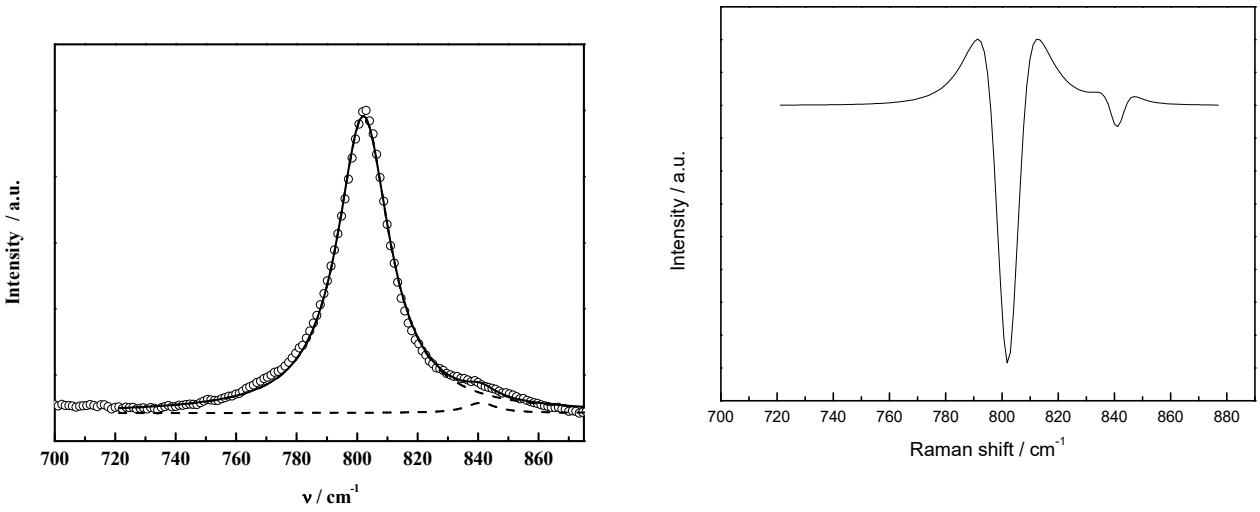

Fig. 8 (Left) Open points show the Raman spectra corresponding of a mixture of two minerals, lines represent the best fitting to a two Gaussian curves. (Right) The second derivate of the Raman spectra.

Figure 9

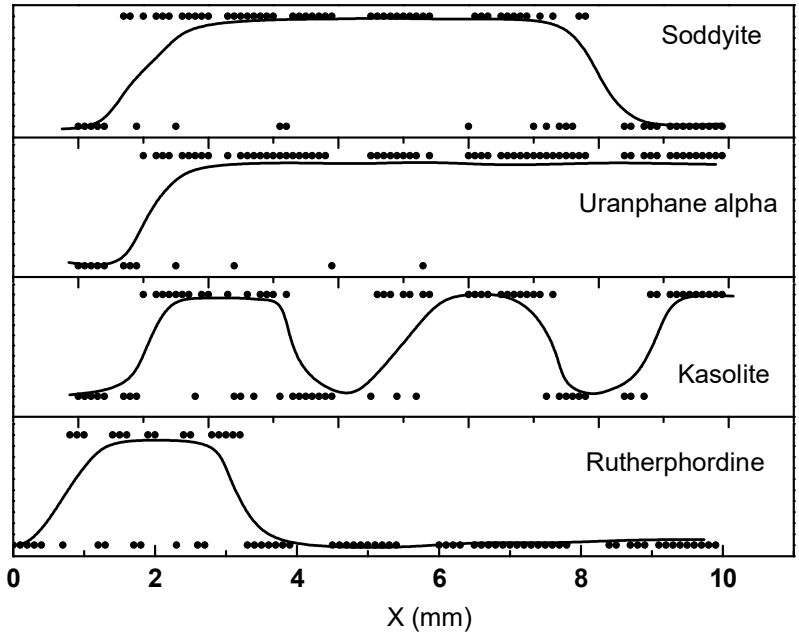

Fig. 9 Points indicate the presence (1) or absence (0) for each analyzed mineral *vs.* position of the analyzed point. Lines indicate the trends of increase or decrease of each phase along the sample.

Tables:

Table 1: Rutherfordine $UO_2(CO_3)$

Band	**Assignation**	**Frequency**	Frequency

		This work	[36]
a	Lattice vibration	142	---
b	Lattice vibration	162	---
c	Lattice vibration	220	---
	$\nu_4(CO_3)^{2-}$	789	799
			784
e	$\nu_2(CO_3)^{2-}$	833	804
f	**$\nu_1(UO_2)^{2+}$**	**889**	866
g	$\nu_1(CO_3)^{2-}$	1120	1115

Table 2 Uranophane alpha $Ca(UO_2)_2(SiO_3OH)_2 \cdot 5H_2O$

Band	**Assignation**	**Frequency**	Frequency

		This work	[37]
a	Lattice vibration	170	166.7
b	$\nu_2(UO_2)^{2+}$	209	213.7
c	$\nu_2(UO_2)^{2+}$	254	250.3
d	$\nu_2(UO_2)^{2+}$	300	306.5
			288.9
			280.5
e	$\nu_2(SiO_4)^{4-}$	403	398.9
f	$\nu_4(SiO_4)^{4-}$	473	469.5
g	$\nu_4(SiO_4)^{4-}$	547	544.6
h	$\nu_1(UO_2)^{2+}$	798	796.9
i	**$\nu_1(SiO_4)^{4-}$**	**967**	963.9

Table 3: **Soddyite** $(UO_2)_2SiO_4 \cdot 2H_2O$

Band	**Assignation**	**Frequency** This work	Frequency [38]
a	Lattice vibration	107	111

b	$\nu_2(UO_2)^{2+}$	195	190
c	$\nu_2(UO_2)^{2+}$	225	229
d	$\nu_2(UO_2)^{2+}$	293	290
	$\nu_2(UO_2)^{2+}$	312	310
	$\nu_2(SiO_4)^{4-}$	404	--
e	$\nu_4(SiO_4)^{4-}$	463	459
f	**$\nu_1(UO_2)^{2+}$** + **$\nu_1(SiO_4)^{4-}$**	**832**	828

Table 4: **Kasolite** $PbUO_2SiO_4 \cdot H_2O$

Band	**Assignation**	**Frequency** This work	Frequency [31]

a	Lattice vibration	107	107.5
b	$\nu_2(UO_2)^{2+}$	217	217.7
c	$\nu_2(UO_2)^{2+}$	237	234.3
d	$\nu_2(SiO_4)^{4-}$	424	454.6
			415.1
e	$\nu_2(SiO_4)^{4-}$	553	550.4
f	**$\nu_1(UO_2)^{2+}$**	**768**	766.7
g	**$\nu_1(SiO_4)^{4-}$**	**912**	903.6